JCTC Journal of Chemical Theory and Computation

Article

pubs.acs.org/JCTC

A New Quantum Calibrated Force Field for Zinc−Protein Complex

Tong Zhu,[†] Xudong Xiao,[†,‡] Changge Ji,*[,†,‡] and John Z. H. Zhang*[,†,‡,§]

[†]Center for Laser and Computational Biophysics, State Key Laboratory of Precision Spectroscopy, East China Normal University, Shanghai 200062, China

[‡]Institute of Theoretical and Computational Science, Institutes for Advanced Interdisciplinary Research, East China Normal University, Shanghai 200062, China

[§]Department of Chemistry, New York University, New York, New York 10003, United States

Supporting Information

ABSTRACT: A quantum calibrated polarizable-charge transfer force field (QPCT) has been proposed to accurately describe the interaction dynamics of zinc−protein complexes. The parameters of the QPCT force field were calibrated by quantum chemistry calculation and capture the polarization and charge transfer effect. QPCTs are validated by molecular dynamic simulation of the hydration shell of the zinc ion, five proteins containing the most common zinc-binding sites (ZnCys2His2, ZnCys3His1, ZnCys4, Zn2Cys6), as well as protein−ligand binding energy in zinc protein MMP3. The calculated results show excellent agreement with the experimental measurement and with results from QM/MM simulation, demonstrating that QPCT is accurate enough to maintain the correct structural integrity of the zinc binding pocket and provide accurate interaction dynamics of the zinc−residue complex. The current approach can also be extended to the study of interaction dynamics of other metal-containing proteins by recalibrating the corresponding parameters to the specific complexes.

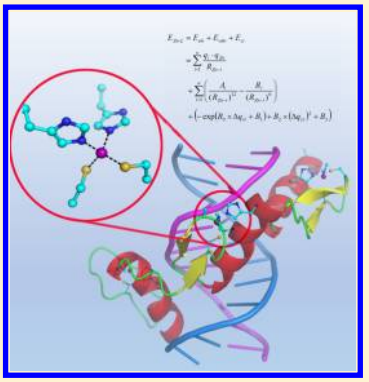

1. INTRODUCTION

Almost half of the proteome of living organisms comprises metalloproteins. Out of various metal cofactors, zinc occupies a prominent place, and it serves both structural and catalytic roles. It has been estimated that ∼10% of the proteins could be zinc proteins, and zinc is the only metal encompassing all six recognized classes of enzymes.[1−11] Due to the important biological function of zinc-containing proteins, molecular modeling is often employed to study their structure and dynamics properties.[12−33] In the past decade, with the development of quantum chemical methods and computer technology, one has seen increased application of QM and QM/MM methods in the calculation of zinc proteins.[34−39] However, due to heavy computational cost, these methods are severely limited in their applications to large protein systems or long time simulation such as conformation sampling and structure refinement etc. For these tasks, molecular mechanics (MM) is still the dominant approach. However, the success of MM methods relies heavily on the accuracy of the force fields employed.[40,41] Unfortunately, the existing force fields are generally incapable of properly describing metalloproteins, and this has already become a practical obstacle for molecular modeling studies of metalloproteins.

At present, there are three general classes of force field for zinc or other metal-containing proteins: the *bonded* model, *cationic dummy atom* model, and *nonbonded* model. In the bonded model, explicit harmonic like energy terms for the bond length and bond angle are introduced into the potential energy function to account for the binding between metal ion and its ligands.[40,42−47] The main feature of bonded models is that the metal binding structure is preserved by the nature of the energy function. The cationic dummy atom model[48−50] places virtual fractional charges around zinc to mimic valence electrons. Previous studies of Pang and co-workers[48−52] show that, using this model, the tetra-coordination of zinc binding group (ZBG, contains the zinc ion and protein residues in its first coordination shell) can be maintained during simulation and enabled some of the first realistic MD simulations for several Zn enzymes. In the nonbonded model, the interaction between metal and its ligands is represented by van der Waals and electrostatic terms. The nonbonded model avoids the conformational restriction of the bonded models and should be more appropriate for studying the interaction dynamics of metalloprotein complexes.[16,21,53−57] However, attempts to use such nonbonded models have encountered problems stemming primarily from the difficulty in correctly treating strong electrostatic interactions of the divalent ion. Previous studies showed that the structure of a metal protein may distort severely in the standard force field with an integer charge assigned to the zinc. Actually, due to the long-range nature of electrostatic forces, the zinc ion tends to get close to any negatively charged amino acid residues. A number of experimental and theoretical studies have demonstrated the importance of long-range protein−ion interactions where significant contributions come from distances as large as 15

Received: December 12, 2012
Published: February 15, 2013

Å.[58,59] Even the zinc binding moiety is preserved; the inaccurate atom charge of zinc ions still can significantly affect the overall protein structure after long-time simulation.

Numerous studies have suggested that, to accurately investigate the effects of long-range electrostatic interactions on the binding of the metal ion in proteins, it is essential to include polarization and the charge transfer effect in potential energy function models.[17,56,60,61] For the bonded model, as the initial bonded structure is highly preserved, the predefined RESP charge of the zinc-binding moiety can be easily adopted.[45] For the nonbonded model, the structure of the zinc-binding moiety fluctuates; thus the structure-dependent polarization and charge transfer models must be taken into account. SIBFA[62−72] was one of the first potentials developed to model zinc interaction with biological molecules by rigorously incorporating polarization, charge transfer, penetration, and other effects. Although the parametrization process of SIBFA is relatively complex, it can give very accurate ion−ligand interaction energies, comparable to high-level *ab initial* methods. Sakharov and Lim introduced distance-dependent partial charges on zinc to consider the polarization and charge transfer effect (CTPOL).[55,56] MD simulation using this model reproduced the experimentally observed tetrahedral structures of Cys2His2, Cys4, and even multi-ion zinc binding sites in proteins. Ren et al. also took into account the polarization effect with the AMOEBA[21,73] model, and their MD simulation of the Cys2His2 zinc finger and a zinc enzyme has yielded reasonable results. In a previous work, we presented a theoretical approach that includes charge transfer and polarization for dynamics studies of metalloproteins based on a recently developed adaptive polarized protein-specific charge (APPC).[74] In this method, the zinc binding group is treated as a special fragment. In MD simulation using APPC, quantum calculation of the ZBG fragment is performed periodically to update its charge redistribution. On the basis of this method, the structure and dynamics of a recently designed dizinc metalloprotein (DFsc) was shown to be correctly described. However, the repeated quantum mechanical calculation is computationally demanding for long-time MD simulation.

Recently, we developed a new Semifluctuating Charge Model[75] (SFC) to account for the polarization effect in biomolecules. The parameters in this model were derived from large sets of quantum electronic structure calculation of model systems in the gas phase and in solution. The polarization effect is explicitly included in this model since charges used were updated frequently according to the local electrostatic environment during MD simulation while demanding a relatively small computational cost. Here, we combine the SFC model with a charge transfer model to describe the zinc−ligand interaction in zinc proteins.

The paper is organized as follows: In the next section, we describe the potential energy function used to describe zinc−ligand interactions in metalloprotein and the parametrization process. Then, dynamics and structures of several model systems were studied to validate the new force field. Finally, the new force field is applied to refine the zinc binding complex in protein and to estimate the affinity of ligand binding to zinc protein.

2. THEORETICAL METHODS

Here, we propose a new force field model to include polarization and charge transfer effects for zinc−protein complexes. The new interaction energy function between zinc (Zn) and its ligand (L) takes the following form:

$$E_{Zn-L} = E_{ele} + E_{vdw} + E_{ct} = \sum_{i=1}^{n} \frac{q_i \cdot q_{Zn}}{R_{Zn-i}} + \sum_{i=1}^{n} \left(\frac{A_i}{(R_{Zn-i})^{12}} - \frac{B_i}{(R_{Zn-i})^{6}} \right) + (-\exp(B_0 \times \Delta q_{ct} + B_1) + B_2 \times (\Delta q_{ct})^2 + B_3) \quad (1)$$

The potential energy function includes three energy terms, namely, electrostatic interaction (E_{ele}), van der Waals interaction (E_{vdw}), and charge transfer energy (E_{ct}). The electrostatic interaction (E_{ele}) is given by Coulomb interaction between the atomic charge of a zinc ion and those of its ligand. A conventional 6−12 Lennard-Jones potential is used to represent van der Waals interaction (E_{vdw}), and the parameters from Kollman and Donini[41,76] were used.

In our model, charge transfer and polarization effects were included in determining the partial charges of zinc and its ligand dynamically in simulation, which is different from traditional force fields. In addition, the quantum calibration of the potential energy function is necessary in order to accurately reproduce the quantum mechanical interaction energy of the zinc−protein complex. This is because the zinc−ligand coordination bond has non-negligible covalent features which could not be accurately represented by classical electrostatic and VDW terms alone. Thus, an additional term E_{ct} (the last term in eq 1) is used to account for the QM effect. For simplicity, the term E_{ct} is simply referred to as "charge transfer energy." The parameters of E_{ct} are thus determined by numerically fitting the force field to quantum mechanical energy. A detailed discussion of this energy term is given in section 2.3.

2.1. Semifluctuating Charge Model for Polar Bond. Chemical groups coordinated with zinc can be strongly polarized due to the large positive charge of the zinc ion. To describe the polarization state of these chemical groups, a Semifluctuating Charge Model (SFC)[66] is adopted here. In this model, the polarized dipole is approximately a linear distribution along the polar bond; thus the polarization can be represented by the charge transfer from one atom to the other on the bond. In the SFC model, charges can only fluctuate along a single polar chemical bond, not the entire molecule. Let us take the polarizable group CO as an example. When a CO group is transferred from the gas phase to liquid, the polarization process can be mimicked as a process of transferring Δq_{pol} from atom O to atom C. Thus, the partial charge on each atom of the final state becomes

$$q_C = q_C^0 + \Delta q_{pol} \quad (2)$$

$$q_O = q_O^0 - \Delta q_{pol} \quad (3)$$

where q_C^0 and q_O^0 are gas phase partial charges on atoms C and O, respectively. The charge transfer due to polarization along the CO bond under a given electric field generated by the environment can be derived [ref 66]:

$$\Delta q_{pol} = \frac{(\Phi_C - \Phi_O)}{2 d_{CO}^2 k_{CO}} \quad (4)$$

where Φ_C and Φ_O are the electrostatic potential at the C and O atoms, respectively. d_{CO} is the C−O bond length, and k_{CO} is the polarizability of the CO group. Details of the derivation of eq 4 and the parametrization process can be found in ref 66. Under this SFC model, the polarization effect of all the polar bonds in the protein can be included and taken into account in the MD simulation. In Table 1, we list the SFC parameters of the common polar groups coordinated to the zinc ion.

Table 1. Parameters of the Polar Groups in Most Common Zinc Binding Residues in QPCT Model[a]

res	bond	$q^0(e)$		k (kcal/mol·debye^2)	d (Å)
Asp	C^γ−O^δ	0.741	−0.772	3.28	1.26
Glu	C^δ−O^ϵ	0.726	−0.779	3.28	1.26
Cym	C^β−S^γ	−0.200	−0.926	1.73	1.81
Hid	N^δ−H^δ	−0.362	0.346	8.76	1.01
HID	C^ϵ−N^ϵ	0.161	−0.528	3.27	1.31
Hie	N^δ−C^ϵ	−0.521	0.141	2.73	1.32
HIE	N^ϵ−H^ϵ	−0.284	0.338	9.70	1.01
water	Ow−Hw	−0.790	0.385	8.46	0.96

[a]The d and k are, respectively, the bond length and the polarizability of the polar group, and $\mathbf{q^0}$ is the partial atomic charge in the gas phase. Details of the derivation of the parameterization process can be found in ref 66.

2.2. Charge Transfer from Zn^{2+} → Ligand. When a coordinate bond forms, the electron density distribution around zinc and its ligands will be distorted and overlap, resulting in charge transfer from the zinc to ligands. Thus, it is critical to include the charge transfer effect in the force field to accurately describe zinc−ligand interaction and to correctly describe the electrostatic interaction between the zinc-binding group and the rest of the protein and solvents. Adapting charge distribution on the zinc binding site by QM calculation has also been performed in previous studies.[16,44,45]

Let us take the ZnCys2His2 zinc binding group as an example. The active site pocket, namely, the zinc ion and its first ligand shell, is extracted from the PDB structure (PDB ID: 1AAY). The side chains of His and Cys are modeled by imidazole (Im) and ethylthiolate (Et), as shown in Figure 1. The geometry of $[Zn(Et)_2(Im)_2]^0$ is then fully optimized by quantum calculation at the B3LYP/6-311++G(2df,p) level. By varying the Zn−S distance and keeping the other geometries of the system fixed, we obtained NBO charges of each atom along the reaction coordinate at the MP2/6-311++G(2df,p) level. The total NBO charge of ethylthiolate was used to calculate the amount of charge transfer (i.e., Δq_{ct} = total charge of Et in coordination complex − total charge of Et in the gas phase). The calculated charge transfer from the zinc ion to Et is shown in Figure 2. For comparison, the charge transfer from the zinc ion to Et in the ZnCys4 and ZnCys3His1 complexes is also shown. In this study, the amount of charge transfer (Δq_{ct}) from the zinc ion to its donor atom can be fitted into the following function:

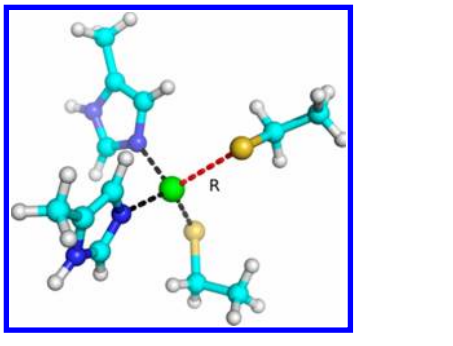

Figure 1. Model system $[Zn(Et)_2(Im)_2]^0$ representing the ZnCys2His2 binding structure used in fitting the charge transfer and binding energy as a function of the distance between zinc and the ligated atom.

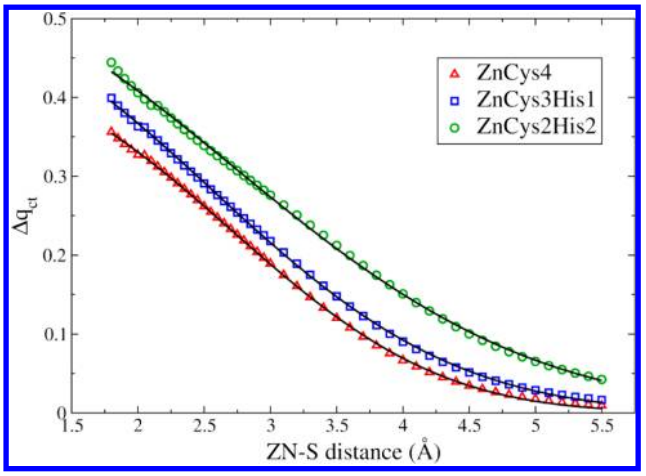

Figure 2. QM calculated charge transfer (Δq_{ct}, NBO charge) at the MP2/6-311++g(2df,p) level as a function of the coordinate bond length for ethylthiolate in ZnCys2His2, ZnCys4, and ZnCys3His1 systems. Solid lines denote analytical fitted curves of QM results.

$$\Delta q_{ct} = A_0 \times \exp[-(R_{Zn-L}/A_1)^{A_2}] \quad (5)$$

where R_{Zn-L} is the coordination bond length and A_0, A_1, and A_2 are parameters used in least-squares fitting to QM calculated results. As shown in Figure 2, the total amount of charge transfer from Zn to S is significant; it is nearly 0.4e for Cys in the equilibrium structure of the ZnCys2His2 model ($R_{Zn-S} \approx 2.3$ Å). In addition, we find that the zinc ion transfers quite different charge amounts to the S atom in different zinc binding complexes. Because the ability to donate electrons from S and N atoms to zinc ions is different, as the number of S atoms increases, the amount of charge transfer from zinc to each individual S atom decreases. Thus, the assumption in ref 50 that the zinc transfers the same amount of charge to the Cys residue in both the ZnCys2His2 and ZnCys4 models is not accurate. It is thus necessary to derive the charge transfer parameters that are specific to the particular zinc binding complex. Such nonadditivity of the charge transfer effect in polyligated metal binding groups was also found previously.[17,45,60]

After Δq (due to both polarization and charge transfer) is computed, the atomic charges of the zinc ion and atoms in the polar groups of protein can be determined as follows

$$q_{Zn} = 2.0 - \sum_{m=1}^{M} \Delta q_{ct}^{m} \quad (6)$$

$$q_i = q_i^0 + \Delta q_{ct} + \Delta q_{pol} \quad (7)$$

where M is the coordination number of the zinc ion. In the SFC model, all of the N−H, C−O, O−H, S−H, and C−N bonds are treated as polar groups, and charges of atoms on these groups are adjusted by Δq_{pol}. In addition, atoms bonded to the zinc ion have Δq_{ct}. For all other atoms, $\Delta q_{pol} = \Delta q_{ct} = 0$.

2.3. Charge Transfer Energy. Since a large amount of charge transfer occurs between the zinc ion and its coordinated ligand, classical electrostatic interaction between the zinc ion and the ligand is greatly reduced. The reduction of the electrostatic energy is compensated by the valence energy of the bond, which is quantum mechanical in nature. Thus, to accurately reproduce the bonding energy, an extra energy term is needed for zinc−ligand interaction in the force field, in addition to the classical electrostatic and van der Waals energy terms. To implement this, quantum mechanically determined interaction energy between Et and $[Zn(Et)_1(Im)_2]^{+1}$ was used to calibrate charge transfer energy in eq 1. As shown in Figure 3, the charge transfer energy (E_{ct}), as a function of charge

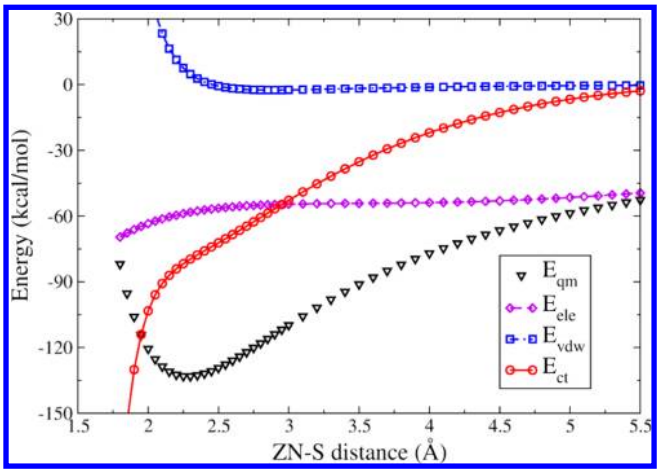

Figure 3. Interaction energies of ethylthiolate (Et) and $[Zn(Et)(Im)_2]^{+1}$ as a function of coordinate bond length. E_{qm} is the binding energy of Et and the $[Zn(Et)(Im)_2]^{+1}$ calculated by Gaussian09 at the MP2/6-311++g(2df,p) level. E_{ele} is the electrostatic interaction between Et and the $[Zn(Et)(Im)_2]^{+1}$. E_{vdw} is the van der Waals interaction energy between Et and the $[Zn(Et)(Im)_2]^{+1}$, and E_{ct} is "charge transfer" energy between Et and the $[Zn(Et)(Im)_2]^{+1}$ ($E_{ct} = E_{qm} - E_{ele} - E_{vdw}$).

transfer Δq_{ct}, is fitted to calculated quantum mechanical energies using the following function

$$E_{ct} = -\exp(B_0 \times \Delta q_{ct} + B_1) + B_2 \times (\Delta q_{ct})^2 + B_3 \quad (8)$$

where B_0, B_1, B_2, and B_3 are parameters determined by numerical fitting. E_{ct} is only added to interaction between zinc and its ligated atom.

It should be noted that the energy terms (E_{ele}, E_{vdw}, and E_{ct}) used in the potential energy function list above are all "effective" energies; thus there are no equivalent relations between energy components in this function with the QM method. Many contributions of QM energy such as coulomb, exchange, correlation, polarization, and charge-transfer are implicitly included in these effective energy terms.

In addition, eq 1 is calibrated to the interaction energy of one ligand with the complex formed between zinc and the other three ligands, with the assumption that the zinc binding group will not undergo large changes during the simulation, and the fluctuation of the coordination geometry can be averaged. Thus, the charge transfer and E_{ct} have cut off when the coordinate bond distance becomes larger than the sum of the VDW radius of zinc and its ligated atom. However, due to the highly nonadditive nature of the zinc binding moiety,[63−65] this equation cannot reproduce the total interaction energy of the $Zn(ligand)_4$ complex (see Table 4 in ref 67). Thus, this model is not intended to represent the energetics of processes involving coordination number rearrangement or the insertion−extraction mechanism of zinc into the protein. To do such work, a more general and precise method like SIBFA[62,67] is needed.

Using the same method as applied to ZnCys2His2, we also parametrized ZnCys3His1, ZnCys4, and ZnHis3Asp1 sites; the parameters can be found in the Supporting Information.

Through combined polarization and the charge transfer effects, a new force field for MD simulation of zinc protein is presented. We call it quantum-based polarizable-charge transfer force field for zinc-binding complexes (QPCT). The validation of QPCT will be provided in the next section.

2.4. Application to Specific Zn−Protein Complexes. In the present study, the hydration of the zinc ion and five zinc proteins containing the most common zinc-binding complexes was studied in molecular dynamic simulations: (1) the classical Cys2His2 type zinc finger peptide which represents the ZnCys2His2 binding site (PDB ID: 1AAY, amino acids 103−135 corresponding to the classical Zn-finger domain); (2) the adenylate kinase representing the ZnCys4 binding site (PDB ID: 1ZIN, amino acides 127−160 corresponding to the active site lid domain); (3) the human PARP-1 zinc finger representing the ZnCys3His1 binding site (PDB ID: 2L30); (4) matrix metallo-protease 3 which represents ZnHis3Asp binding sites (PDB ID: 1HFS); and (5) GAL4 peptide which represents the Zn2Cys6 binding site (PDB ID: 3COQ). Each of the above protein systems is solvated in an octahedron-like TIP3P water box and is neutralized by adding counterions. Periodic boundary conditions and the particle mesh Ewald method were used to treat long-range electrostatic interaction. Each system is relaxed in 10 000 steps with a constraint on the protein, followed by full minimization with a constraint on the zinc binding group, and then 10 ns simulations without any constraint. For the MD simulation, the integration time step is 1 fs. The temperature is regulated using Langevin dynamics with the collision frequency set to 2 ps^{-1}. All the covalent bonds involving hydrogen atoms are fixed by applying the SHAKE algorithm. After heating and equilibration, the production MD simulation was performed at 300 K (NPT). The environment dependent charge was applied to all the polar groups in the protein. In the current simulation study, a modified version of the Amber12 package is used. To accurately calculate the electrostatic potentials, a self-consistent procedure is necessary. However, since frequent iteration in MD simulation is very time-consuming, the electrostatic potentials on each atom were stored and averaged every 100 time steps during the simulation, and the polarized charges of the polar group are updated according to the time-averaged electrostatic potential over each 100 time-step period. The Δq_{ct} and E_{ct} between the zinc ion and its ligated atom are updated every step.

For comparison, we also performed QM/MM MD simulations for each protein. The QM subsystem, including the zinc ion and residues in the first coordination shell, was treated by the B3LYP functional with the Stuttgart ECP/basis set for the zinc atom and the 6-31G* basis for all other atoms. This level of QM treatment has been extensively tested and applied successfully to describe the zinc coordination shell.[36,37] For each protein, 50 ps MD simulation using QM/MM was performed.

3. RESULTS AND DISCUSSION

3.1. Liquid Structure around Zinc Ion. It is widely accepted that zinc ion−water interaction plays a crucial role in many chemical and biological processes. Thus, the hydration of the zinc ion has been a focus of various experimental and theoretical investigations;[73,76−83] the abundance of experimental studies also makes it a good system for force field validation. The radial distribution function (RDF) between the zinc ion and oxygen atom of water molecules obtained from the 10 ns simulation with the QPCT force field is plotted in Figure 4a.

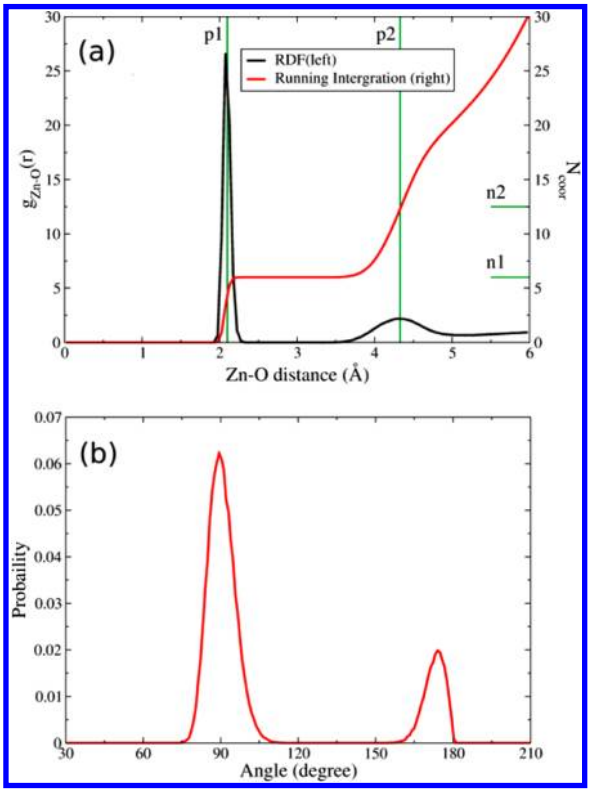

Figure 4. (a) Radial distribution function of Zn−O distance (left *y* axis) and water coordination number (right *y* axis). The p1 and p2 denote, respectively, the peak experimental radial distribution of the first and second solvation shells, while n1 and n2 denote, respectively, the experimental coordination number of the first and second solvation shells. (b) O−Zn−O angle distribution of the zinc ion and the oxygen atom of water in the first solvent shell.

The running integration of Zn−O is also plotted. Two distinct hydration shells can be identified from the RDF of Zn−O, the sharp first peak centered at 2.09 Å, and the running integration indicates a water-coordination number of 6 in the first solvation shell, while the peak of the second solvation shell is at 4.35 Å and running integration indicates a water-coordination number of 12.5. As can be seen, the simulated liquid structure with the QPCT force field agrees well with the experimental measurements.[73,80,82]

In addition to the RDF, the solvation structure has also been analyzed from the distribution of the angles formed by O−Zn−O in the first water shell. Two well-defined peaks can be observed at the peak maxima of 90° and near 180° in the simulation. The running integration numbers show that the area ratio of the two peaks is 4:1. The result indicates that the hydration geometry around the zinc ion is on average a 6-coordinated octahedral, in agreement with many experimental results. The time-dependence (or fluctuation) of atomic charge during the simulation was plotted in Figure S2 in the Supporting Information. The partial charge of zinc is reduced from +2 to about +1.5 during the simulation, indicating that about 0.08*e* was transferred from zinc to a water molecule in the first solvation shell. A value of 0.08*e* is quite a small value since water is a kind of hard base whose ability of giving electrons is relatively weak.

3.2. QPCT Accurately Describes the Structures of Zinc Fingers. In general, zinc fingers coordinate zinc ions with a combination of cysteine and histidine residues while the number and order of these residues are used to classify different types of zinc fingers (e.g., Cys2His2, Cys4, and Cys6). Due to their small and stable structures, zinc fingers are ideal benchmarks for testing the force field for zinc protein. We performed a 10 ns MD simulation with the QPCT force field on a classical Cys2His2 zinc finger protein starting from the X-ray structure 1AAY (as shown in Figure 5). The calculated

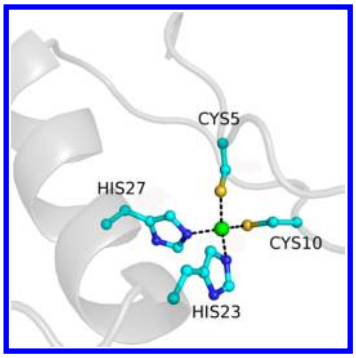

Figure 5. Cartoon representation of the ZnCys2His2 type zinc finger (PDB ID 1AAY). Black dashed line denotes coordination bond.

RMSD of heavy atoms in the protein backbone and zinc binding group was plotted in Figure S3. The RMSD initially rises and then reaches a plateau after 1 ns and fluctuates around a mean value of 1 Å. To check the accuracy of the QPCT force field in describing the local zinc binding structure, we measured the bond angles and bond distances contain zinc ions over the simulation time, as shown in Figure 6, Figure S4, and Table 2. For comparison, the result computed by QM/MM MD is also presented. It is found that the distances between the zinc ion and the atoms ligated to it are very stable during the MD simulation, and their average values show excellent agreement with the QM/MM simulation result and crystal structure. For instance, the simulation with QPCT yields an average Zn−S^{γ}@C5 distance of 2.29 ± 0.07 Å, very close to the results of QM/MM MD (2.32 ± 0.06 Å) and X-ray (2.29 ± 0.10 Å). Other detailed structural parameters can be found in Table 2. Several previous works made extensive surveys of the available zinc binding sets in Protein Data Bank (PDB) and gave the average coordination bond lengths and bond angles containing zinc.[11,45] As can be seen in Table 2, the zinc bond length and bond angle calculated by QPCT show remarkable agreement with the average values reported.[11,45] This clearly demonstrates that the QPCT can accurately describe the interaction of these zinc binding complexes and can be applied to dynamics simulation of proteins containing the same zinc coordinate sphere.

The atomic charges of the ZBG atoms are shown in Table 3. The charge of zinc is reduced to about 1.11*e* in the simulation, which implies that about a 0.9*e* charge is transferred from zinc

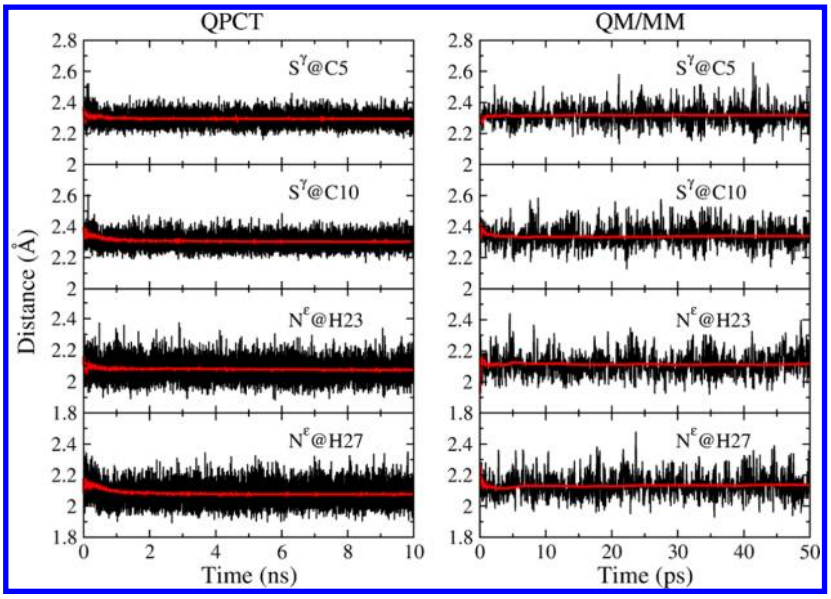

Figure 6. Time-dependence of the coordination bond lengths in ZnCys2His2 type zinc finger peptide. Red lines denote time-averaged values.

Table 2. Comparison of Computed Average Distances and Angles between Zinc and Its Ligated Atoms of the ZnCys2His2 Type Zinc Finger Peptide with Experimental and QM/MM Values (All the Bond Lengths Are in Ångströms and Bond Angles in Degrees)

zinc−ligand geometry[a]	PDB survey[b]	X-ray[c]	MD (10 ns)	QM/MM (50 ps)
Zn−S^{γ}@C5	2.301 ± 0.129	2.29 ± 0.10	2.29 ± 0.07	2.32 ± 0.06
Zn−S^{γ}@C10	2.301 ± 0.129	2.29 ± 0.10	2.30 ± 0.08	2.34 ± 0.07
Zn−N^{ε}@H23	2.088 ± 0.119	2.04 ± 0.08	2.07 ± 0.12	2.12 ± 0.07
Zn−N^{ε}@H27	2.088 ± 0.119	2.04 ± 0.08	2.08 ± 0.12	2.13 ± 0.07
∠(N^{ε}@H23−Zn−N^{ε}@H27)	112 ± 7	105 ± 6	101 ± 13	99 ± 7
∠(N^{ε}@H23−Zn−S^{γ}@C5)	107 ± 7	101 ± 8	110 ± 13	108 ± 7
∠(S^{γ}@C15Zn−S^{γ}@C10)	110 ± 6	117 ± 6	114 ± 10	114 ± 6

[a]Single letter abbreviation for residue is used. [b]Taken from refs 1, 33, and 45. [c]PDB ID 1AAY.

Table 3. Comparison of Time-Averaged Partial Atomic Charges of the First Coordination Shell Residues of the ZBG in ZnCys2His2 Type Zinc Finger in QPCT with Standard Charges in AMBER99SB Force Field

res[a]	atom	QPCT(e)	AMBER99SB(e)
	Zn	1.11	2.00
C5	S^{γ}	−0.78	−0.88
C10	S^{γ}	−0.78	−0.88
H23	N^{ε}	−0.56	−0.57
H27	N^{ε}	−0.56	−0.57

[a]Single letter abbreviation for residue is used.

to its ligated atoms. The partial charge of N^{ε} on His23 and His27 is −0.56e, very close to the value in the AMBER99SB force field (−0.57e), but the S^{γ}'s charge becomes relatively small compared to that of AMBER99SB (−0.78e versus −0.88e), because of the large amount of charge transfer.

In addition to the Cys2His2type zinc finger, we also performed MD simulations by the QPCT method on the classical Cys3His1 and Cys4 zinc finger peptides. The results are shown in the Supporting Information. Overall, both structures are maintained very well during the simulation, the stability of the ZBG is even better in these two systems than that in Cys2His2 zinc finger, and the calculated bond length and angles by QPCT are in excellent agreement with that calculated by QM/MM and experimental measurements. All these results indicate that the QPCT method is very suitable for the long-time simulation of the zinc-protein simulation.

It is also worth it to mention that about 5 days are needed to complete the 10 ns simulation with the QPCT force field, while about 40 days are needed to perform 50 ps simulation QM/MM MD on the same machine. Therefore, for long MD simulation of s large system, QPCT is a very superior choice.

3.3. Protein Environment Is Important for Structure of Zinc Binding Site. Then, we check the performance of the QPCT force field on a zinc binding site containing carboxylate. A martrix metallo-protease 3/inhibitor complex (MMP3) was investigated. There are two zinc binding sites in this protein: one of them is a structural zinc which coordinates to three His and one Asp residue, while the other is a catalytic zinc which coordinates with three His and the inhibitor L04 (see Figure.7). These two zinc sites share similar binding modes: both zinc ions bind to three imidazoles and one carboxylate group. Previous studies demonstrated that over 84% of the Asp/Glu residue binds to the zinc ion with a monodentate carboxylate.[8,84] However, to maintain the monodentate carboxylate binding site during the MD simulation is a really big challenge for a traditional molecular mechanics force field, as the noncoordinated O atom in the carboxyl group is very close to the zinc ion; the strong electrostatic interaction between them greatly reduced their distance. Average structural parameters derived from simulation using the QPCT force field

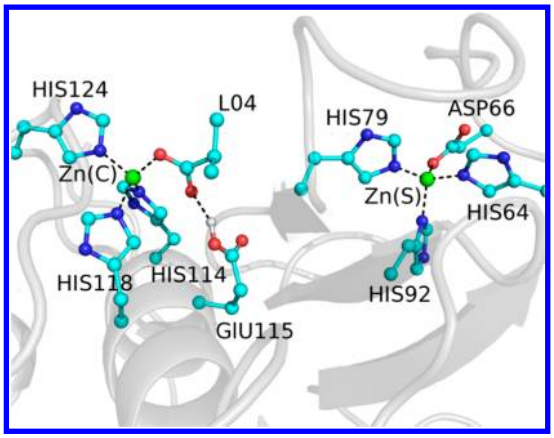

Figure 7. Cartoon representation of MMP3 (PDB ID: 1HFS) and its zinc binding sites. Black dashed lines denote coordination or hydrogen bonds.

are listed in Tables 4 and 5 and Figures S13−15. As can be seen, the structures of the MMP3 are well preserved during the simulation, and the QPCT calculated results agree very well with the experimental and QM/MM MD results.

Table 4. Comparison of Computed Average Distances and Angles between Zinc and Its Ligated Atoms of the MMP3 Protein Consisting of the Zinc Binding Complex of ZnHis3Asp1 with the Experimental and QM/MM Values[a]

zinc−ligand geometry[a]	PDB survey[b]	X-ray[c]	MD(10 ns)	QM/MM (50 ps)
Zn(C)−O^3@ Ligand	2.10 ± 0.16	1.84	2.05 ± 0.12	2.07 ± 0.10
Zn(C)−O^2@ Ligand	3.00 ± 0.37	2.62	2.45 ± 0.27	2.56 ± 0.28
Zn(C)−N^ε@ H114	2.077 ± 0.1275	1.90	1.98 ± 0.09	2.04 ± 0.10
Zn(C)−N^ε@ H118	2.077 ± 0.1275	1.93	1.96 ± 0.08	2.06 ± 0.11
Zn(C)−N^ε@ H124	2.077 ± 0.1275	1.84	1.90 ± 0.09	2.04 ± 0.08
Zn(S)−$O^{\delta2}$@ D66	2.10 ± 0.16	2.00	1.97 ± 0.11	2.07 ± 0.09
Zn(S)−$O^{\delta1}$@ D66	3.00 ± 0.37	3.20	3.35 ± 0.31	3.44 ± 0.24
Zn(C)−N^ε@H64	2.077 ± 0.1275	1.83	1.94 ± 0.05	2.01 ± 0.08
Zn(C)−N^ε@H79	2.077 ± 0.1275	1.78	1.93 ± 0.09	1.98 ± 0.09
Zn(C)−N^δ@H93	2.077 ± 0.1275	2.01	1.95 ± 0.10	2.03 ± 0.09
∠(O^3@Ligand−Zn(C)−N^ε@ H118)	107 ± 12	128	133 ± 13	124 ± 7
∠(N^ε@H114−Zn(C)−N^ε@ H118)	112 ± 7	99	99 ± 11	103 ± 9
∠($O^{\delta2}$@D66−Zn(S)−N^ε@ H64)	107 ± 12	118	113 ± 6	107 ± 6
∠(N^ε@H64−Zn(C)−N^ε@ H79)	112 ± 7	114	108 ± 7	111 ± 7

[a]Single letter abbreviation for residue is used. All the bond lengths are in Ångströms and bond angles in degrees. The zinc ions in the catalytic sites are denoted as Zn(C), while the zinc ions in the structure sites are denote as Zn(S). [b]Taken from refs 1, 33, and 45. [c]PDB ID 1HFS.

Although binding modes are similar for the two zinc sites, the detailed binding structure shows some difference. In the structural zinc site, the distances between carboxylate O atom and zinc ion are 2.05 ± 0.12 Å and 2.45 ± 0.27 Å, respectively. While in the catalytic zinc site, the distances between the carboxylate O atom and zinc ion are 1.97 ± 0.11 Å and 3.35 ± 0.31 Å, respectively. Both carboxylate groups bind with the monodentate binding mode. What is more interesting is that in the QPCT result, even the fluctuation of the Zn−$O^{\delta1}$ distance is very close to that calculated by the QM/MM simulation (see Figure S14). Since both O atoms in the carboxylate group can act as donors when bound to the zinc ion, the final binding mode is determined by local electrostatic environment. In the ZnHis3Asp1 site, the carboxylate group of Asp forms a hydrogen bond with a nearby water molecule. In the ZnHis3L04 site, the carboxylate group of the inhibitor forms a hydrogen bond with Glu115. The difference in local electrostatic environment, especially the secondary coordinate shell around the zinc sites, is the origin of structure variation between the two zinc sites in MMP3. Several other studies also highlighted the role of protein environment in the process of protein−metal interaction and metalloprotein function.[85−87] By including polarization effect, the QPCT method can correctly describe the electrostatic interactions around the zinc ion, which is essential in describing the structure and dynamics of zinc binding sites and the entire protein.

Table 5. Comparison of Time-Averaged Partial Atomic Charges of the First Coordination Shell Residues of the ZBG in MMP3 in QPCT with Standard Charges in AMBER99SB Force Field

res[a]	atom[b]	QPCT(e)	AMBER99SB(e)
	Zn	1.41	2.00
H114	N^ε	−0.59	−0.57
H118	N^ε	−0.58	−0.57
H124	N^ε	−0.58	−0.57
L04	O^3	−0.87	−0.80
L04	O^{2*}	−0.65	−0.80
	Zn	1.45	2.00
H64	N^ε	−0.58	−0.57
H79	N^ε	−0.60	−0.57
H92	N^δ	−0.56	−0.54
D66	$O^{\delta2}$	−0.87	−0.80
D66	$O^{\delta1*}$	−0.74	−0.80

[a]Single letter abbreviation for residue is used. [b]The ∗ denotes O atoms which not coordinate with Zinc ion.

3.4. Refinement of Local Zinc−Protein Structure. Due to limitations of the current molecular force field, the energy-based refinement of X-ray and NMR protein structures to high accuracy remains a challenge in structural biology, especially for the metalloproteins. Thus, there are many "*poor*" zinc coordinate geometries in the Protein Data Bank. For example, the dizinc metal site in the crystal structure of a Gal4 protein (shown in Figure 8), defined by Hong et al.[88] at a resolution of 2.4 Å, was ill defined. The distance between zinc and S^γ@ CYS14 is only 1.89 Å, which is too short for the normal Zn−S coordinate bond. Compared to the bonded model,[44,45] the nonbonded scheme of the QPCT method includes enough flexibility to allow for small structural rearrangements of the zinc binding site; thus it may be used for the refinement of zinc protein structures. In this study, we derived QPCT parameters from the Zn2Cys6 model system and used them in simulation of the Gal4 protein. The refined key structural parameters such as bond lengths and bond angles were listed in Table 6. For comparison, results derived from the QM/MM simulation are

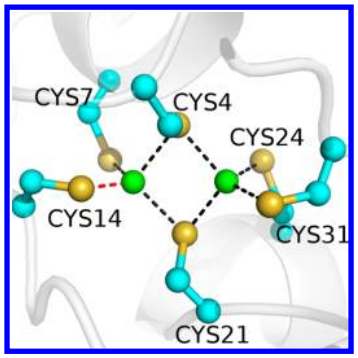

Figure 8. Cartoon representation of GAL4 (PDB ID 3COQ) and one of its dizinc metal sites. One of the coordination bonds between zinc and the S atom is only 1.89 Å (represented by red dashed line).

also listed in Table 6. As can be seen, the obtained Zn−S distance and S−Zn−S angles from QPCT and QM/MM simulations are in close agreement with each other. All the Zn−S bond lengths range from 2.3 Å to 2.5 Å, which is very reasonable. In the zinc binding site, two types of sulfur atoms can be distinguished: a "*terminal*" sulfur atom, S_t, coordinated to one Zn ion and a "*bridging*" sulfur atom, S_b, coordinated to two Zn ions.[51] The geometric and electronic characters of these two types of S atom are different. The average distance from Zn to S_t is shorter than that to S_b in our simulation study. Partial charges on S_t and S_b atoms are also different, since the charge on S_b was transferred to two zinc atoms while that on S_t was transferred only to one zinc atom. The average charge on S_b and S_t is about −0.71*e* and −0.81*e*, respectively (see Table 7).

Table 6. Calculated Average Distance and Angles between Zinc and Its Coordinate Atoms of the GAL4 Peptide Compared with Experimental and QM/MM Values (All the Bond Values Are in Ångströms and the Angle Values in Degrees)

zinc−ligand geometry[a]	X-ray[b]	MD (10 ns)	QM/MM (50 ps)
Zn1−Zn2	3.22	3.38 ± 0.23	3.38 ± 0.24
Zn1−S$^{\gamma}$@C4	2.49	2.46 ± 0.09	2.53 ± 0.14
Zn1−S$^{\gamma}$@C7	2.32	2.35 ± 0.08	2.32 ± 0.11
Zn1−S$^{\gamma}$@C14	2.38	2.35 ± 0.08	2.42 ± 0.12
Zn1−S$^{\gamma}$@C21	2.52	2.46 ± 0.10	2.47 ± 0.09
Zn2−S$^{\gamma}$@C4	2.32	2.45 ± 0.11	2.41 ± 0.13
Zn2−S$^{\gamma}$@C21	2.58	2.46 ± 0.08	2.65 ± 0.10
Zn2−S$^{\gamma}$@C24	1.89	2.35 ± 0.07	2.31 ± 0.11
Zn2−S$^{\gamma}$@C31	2.31	2.35 ± 0.09	2.38 ± 0.13
∠(Zn1−S$^{\gamma}$@C4−Zn2)	83	88 ± 7	82 ± 6
∠(Zn1−S$^{\gamma}$@C21−Zn2)	78	88 ± 7	86 ± 5
∠(S$^{\gamma}$@C7−Zn1−S$^{\gamma}$@C14)	109	118 ± 12	122 ± 8
∠(S$^{\gamma}$@C24−Zn2−S$^{\gamma}$@C3)	90	116 ± 12	116 ± 8

[a]Single letter abbreviation for residue is used. [b]PDB ID 3COQ.

A foremost concern in the simulation of proteins containing multizinc binding sites is the distance between zinc ions, since the electrostatic interaction is very strong between two ions with large positive charges. Thus, a successful simulation is dependent on the accuracy of the force field. As can be seen from Table 6, the calculated zinc−zinc distance by QPCT is very close to the X-ray value and is in excellent agreement with that from the QM/MM calculation. However, the distance between two zincs calculated with the AMBER99SB force field is obviously much longer than that of QPCT and QM/MM, as shown in Figure S18. Further analysis of the trajectories generated by MD with the AMBER99SB force field shows that the overall structure of the protein and the zinc binding site have been distorted; there are two waters coordinated to the first zinc ion and the backbone O atom of Leu3 bound to another zinc ion (see Figure 9). Since large amounts of charge were transferred from zinc to the ligand atoms, the net charges of the zinc ions were significantly reduced from 2.0*e* to 1.02*e*. Thus, without considering the charge transfer effect, the repulsive electrostatic force between two zinc atoms will be grossly overestimated (about 4 times stronger). Such strong overestimation of repulsion can cause expansion of the dizinc sites in the simulation and distort the overall protein structure. These results suggest that including the charge distribution of the zinc binding group in the force field is essential to correctly describing multimetal sites in the protein.

Table 7. Comparison of Time-Averaged Partial Atomic Charges of the First Coordination Shell Residues of the ZBG in GAL4 in QPCT with Standard Charges in AMBER Force Field

res[a]	atom	QPCT(*e*)	AMBER99SB(*e*)
	Zn	1.12	2.00
	Zn	1.12	2.00
C4	Sγ	−0.71	−0.88
C7	Sγ	−0.82	−0.88
C14	Sγ	−0.81	−0.88
C21	Sγ	−0.71	−0.88
C24	Sγ	−0.81	−0.88
C31	Sγ	−0.81	−0.88

[a]Single letter abbreviation for residue is used.

3.5. Estimation of the Binding Affinity of a Ligand Binding to Zinc Protein. In the past two decades, there has been increasing interest in zinc-containing proteins relating to a variety of human diseases, such as cancer, rheumatoid arthritis, etc. To accelerate the drug design process "*in silico*," it is important to accurately predict the binding affinities of the ligand/inhibitor for zinc-containing proteins. However, modeling of the ligand binding to the zinc protein is problematic, especially for ligands which directly ligate to the zinc ion, because of the complicated nature of the metal coordinate interaction.[41,89−92]

In a previous study, Kollman and co-workers tried to compute the binding affinity of matrix metalloproteinases 3(MMP3) and its inhibitors through a MD simulation and MM-PBSA method using the AMBER94 force field.[41] However, they failed to obtain the correct protein/ligand complex structure since the coordinate geometry of experimental structure cannot be reproduced in the simulation due to inaccuracy of the AMBER94 force field. In a previous subsection above, we successfully produced the experimental zinc binding site of the MMP3/inhibitor complex in MD simulation using the QPCT force field. Therefore, in this section, we try to calculate the binding free energy of the MMP3 system based on the MM-PBSA method under the QPCT force field.

The thermodynamic cycle to compute protein−ligand binding as shown in Figure 10 was used to calculate the binding free energy of the ligand to MMP3. In the MM-PBSA method, the free energy of complex formation in solution was decomposed into gas-phase interaction energy ΔG_{gas}^{bind} and a solvation free energy ΔG_{sol}. In the standard application of the

dx.doi.org/10.1021/ct301091z | J. Chem. Theory Comput. 2013, 9, 1788−1798

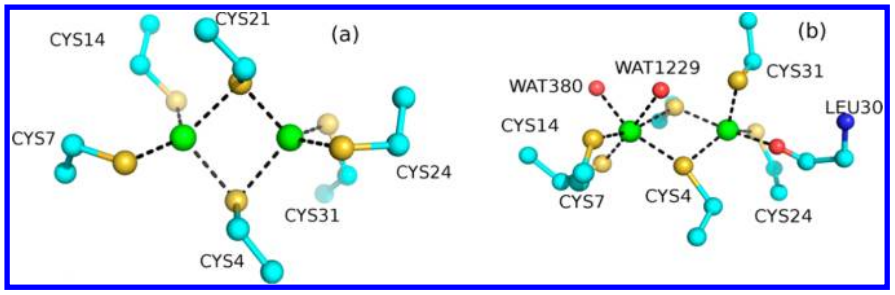

Figure 9. Final structures of the zinc binding group of GAL4 from MD simulation using, respectively, the force field of (a) QPCT and (b) AMBER99SB.

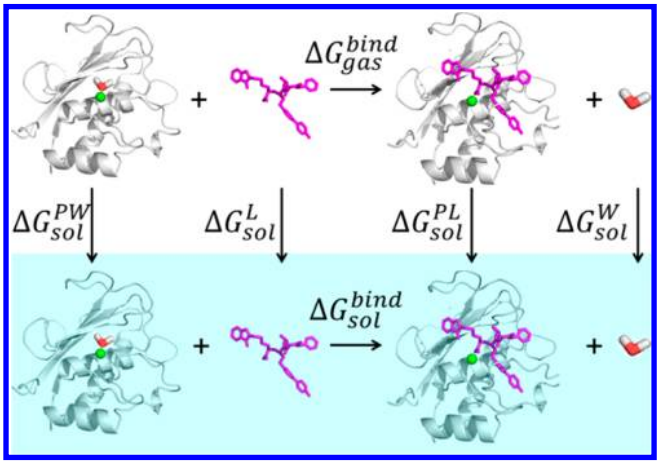

Figure 10. Thermodynamic cycle used to calculate the binding free energy between the protein and ligand during complexation. ΔG_{sol}^{PW} is the solvation energy of the protein-explicit water complex. ΔG_{sol}^{L} is the solvation energy of the ligand. ΔG_{sol}^{PL} is the solvation energy of the protein−ligand complex, and ΔG_{sol}^{W} is the solvation energy of the explicit water. ΔG_{gas}^{bind} is the free energy of binding in the gas phase, and ΔG_{sol}^{bind} is the free energy of binding in solution.

MM-PBSA method, the Poisson−Boltzmann (PB) equation is used to implicitly treat the solvent effect. However, in the *apo* state of MMP3, a water molecule is bound to the zinc ion in the active site due to coordination interaction. This water molecule is thus treated explicitly as part of the protein system in our calculation.

Each energy term calculated using the MM-PBSA method can be summarized in the following set of equations:

$$\Delta G_{sol}^{bind} = \Delta G_{gas}^{bind} + \Delta G_{sol} \quad (9)$$

$$\Delta G_{sol} = \Delta G_{solv}^{PL} + \Delta G_{solv}^{W} - \Delta G_{solv}^{PW} - \Delta G_{solv}^{L} \quad (10)$$

$$\Delta G_{gas}^{bind} = \Delta H_{gas}^{bind} - T\Delta S \quad (11)$$

$$\Delta H_{gas}^{bind} = E^{PL} + E^{W} - E^{PW} - E^{L} \quad (12)$$

$$T\Delta S = T\Delta S^{PL} + T\Delta S^{W} - T\Delta S^{PW} - T\Delta S^{L} \quad (13)$$

A total of 100 conformations of the MMP3/inhibitor complex were extracted from the 10 ns simulation at an interval of every 100 ps, and another 100 conformations of the protein−water complex were obtained by mutating the ligand to a water molecule while the rest of the protein atoms were kept fixed. The QPCT parameters for the ZnHis3Water complex are derived from *ab initio* calculation. The desolvation energy was calculated by DELPHI5.0,[93] and the entropy loss during protein−ligand binding is calculated by normal-mode analysis using the NMODE module in AMBER12. The final result is shown in Table 8. The binding free energy calculated by a QPCT force field is −16.07 kcal/mol, quite close to the experimental measurement (−11.89 kcal/mol). This result shows remarkable improvement to the previous calculation result using standard Amber94 force fields (+19.8 kcal/mol, see ref 41).

Three advantages of our QPCT force field in calculating protein−ligand binding energy for the MMP3 system can be summarized here: First, the local tetrahedral coordination structure is correctly maintained during the simulation. Second, compared to the bonded model, the interaction energy between zinc and the ligand was calibrated by quantum calculation and is thus much more accurate. Third, as the polarization of the protein was taken into account in the QPCT force field, the interaction between polar groups in the binding pocket and the ligand is also more accurately treated.

Due to the limitations of the QPCT and MM-PBSA method, this combination cannot be counted on to predict absolute binding energy with "chemical accuracy." Our hope is that the QPCT method may be used to accurately predict the *relative* protein−ligand binding affinities, but this needs extensive tests and further development. Corresponding studies are ongoing. Of course, further improvement and more extensive study of different systems are needed. The relative work is ongoing in our laboratory.

CONCLUSION

In the current work, a nonbonded quantum-calibrated polarizable-charge transfer force field (QPCT) is proposed to accurately describe the interaction energy of zinc-binding complexes in proteins. This QPCT approach has the following

Table 8. Comparisons of MM-PBSA Binding Energy Using the QPCT Force Field with Experimental Value and with Result from Prior Calculation Using Amber Force Field (ff94) (All Values Are in kcal/mol with Standard Deviation over 100 Snapshots within the Last 10 ns of MD Simulation)

ligand	ΔH_{gas}^{bind}	ΔG_{sol}	$-T\Delta S$	ΔG_{sol}^{bind}	exptl[a]	Amber[b]
L04	−223.5 ± 7.7	182.1 ± 8.2	25.3 ± 4.5	−16.1 ± 3.2	−11.9	+19.8

[a]Calculated from experimental K_i values obtained from Esser's previous work (*J. Med. Chem.* **1997**, *40*, 1026). [b]Obtained from ref 41.

features: (1) The polarization state of all the polar groups in the system are determined by its local electrostatic environment created by the protein and the solvent; thus the long-range electrostatic interaction in the system is accurately treated. (2) The quantum nature of the charge transfer energy in the zinc coordination bond is given by an analytical energy function whose parameters are fitted to zinc binding energy potential from *ab initio* calculation at the MP2/6-311++g(2df,p) level. (3) The functions used in the QPCT force field are easier to parametrize and less computationally expensive. Actual calculation showed that it only demands about 1% extra computational cost compared to using a standard non-polarizable force field during the simulation. (4) The parametrization of the QPCT framework was tested with a range of zinc−proteins containing different metal binding sites. The calculated results clearly demonstrated that by including the polarization and charge transfer effect, the present approach can accurately maintain the integrity of the zinc binding pocket during extended molecular dynamic simulations. In particular, the new force field shows excellent results in refining the zinc−protein structure and calculating protein−ligand binding affinity.

However, while summarizing the successes, we also find some shortcomings in this model: First, to be consistent with the classical force field, the potential energy function in the QPCT method is empirical and not based on the perturbation and variational theories. Second, the QPCT method cannot represent the fully nonadditive nature of the coordinate interaction and thus cannot be used to describe the formation and breaking of more than one coordinate bond or large conformational change of the zinc binding site. To overcome these shortcomings, further parametrization and more energy and structure tests are needed in the further development. However, despite these shortcomings, the current QPCT force field can be readily applied in many aspects for zinc−proteins, such as drug design, generation of dynamical structures of zinc−proteins, de novo zinc protein design, refinement of zinc−protein structures, etc.

■ ASSOCIATED CONTENT

Supporting Information

Several additional tables and figures providing additional data and information from our calculations for further detailed analysis and comparison are provided. This information is available free of charge via the Internet at http://pubs.acs.org

■ AUTHOR INFORMATION

Corresponding Author

*E-mail: chicago.ji@gmail.com, john.zhang@nyu.edu.

Notes

The authors declare no competing financial interest.

■ ACKNOWLEDGMENTS

We thank the National Natural Science Foundation of China (Grant Nos. 21003048, 10974054, and 20933002). C.J. is also supported by "the Fundamental Research Funds for the Central Universities" and Open Research Fund of the State Key Laboratory of Precision spectroscopy, East China Normal University. C.J. thanks Dr. John D. Chodera for his generous help on modifying the Amber source code. We also thank the Computer Center of ECNU for providing us computational time.

■ REFERENCES

(1) Peters, M. B. *The application of semiempirical method in drug design*. Ph.D. thesis, University of Florida, Gainesville, FL, 2005.
(2) Maret, W. *J. Inorg. Biochem.* **2012**, *111*, 110−116.
(3) Andreini, C.; Bertini, I. *J. Inorg. Biochem.* **2012**, *111*, 150−156.
(4) Maret, W.; Li, Y. *Chem. Rev.* **2009**, *109*, 4682−4707.
(5) Auld, D. S. *Biometals* **2001**, *14*, 271−313.
(6) Patel, K.; Kumar, A.; Durani, S. *Biochim. Biophys. Acta, Proteins Proteomics* **2007**, *1774*, 1247−1253.
(7) Andreini, C.; Bertini, I.; Cavallaro, G. *PLoS One* **2011**, *6*, e26325.
(8) Tamames, B.; Sousa, S. F.; Tamames, J.; Fernandes, P. A.; Ramos, M. J. *Proteins* **2007**, *69*, 466−475.
(9) Maret, W. *J. Anal. At. Spectrom.* **2004**, *19*, 15−19.
(10) Sousa, S. F.; Lopes, A. B.; Fernandes, P. A.; Ramos, M. J. *Dalton Trans.* **2009**, 7946−7956.
(11) Lee, Y.-m.; Lim, C. *J. Mol. Biol.* **2008**, *379*, 545−553.
(12) Banci, L. *Curr. Opin. Chem. Biol.* **2003**, *7*, 143−149.
(13) Zimmer, M. *Coord. Chem. Rev.* **2009**, *253*, 817−826.
(14) Hu, L.; Ryde, U. *J. Chem. Theory Comput.* **2011**, *7*, 2452−2463.
(15) Tjornhammar, R.; Edholm, O. *J. Chem. Phys.* **2010**, *132*, 205101−205109.
(16) Sternberg, U.; Koch, F. T.; Brauer, M.; Kunert, M.; Anders, E. *J. Mol. Model.* **2001**, *7*, 54−64.
(17) Dal Peraro, M.; Spiegel, K.; Lamoureux, G.; De Vivo, M.; DeGrado, W. F.; Klein, M. L. *J. Struct. Biol.* **2007**, *157*, 444−453.
(18) Li, W.; Zhang, J.; Wang, J.; Wang, W. *J. Am. Chem. Soc.* **2008**, *130*, 892−900.
(19) Chakravorty, D. K.; Wang, B.; Lee, C. W.; Giedroc, D. P.; Merz, K. M., Jr. *J. Am. Chem. Soc.* **2012**, *134*, 3367−3376.
(20) Wu, R.; Cao, Z.; Zhang, Y. *Prog. Chem.* **2012**, *24*, 1175−1184.
(21) Zhang, J.; Yang, W.; Piquemal, J.-P.; Ren, P. *J. Chem. Theory Comput.* **2012**, *8*, 1314−1324.
(22) Chang, S.; Jiao, X.; Hu, J.-P.; Chen, Y.; Tian, X.-H. *Int. J. Mol. Sci.* **2010**, *11*, 4014−4034.
(23) Lee, J.; Kim, J.-S.; Seok, C. *J. Phys. Chem. B* **2010**, *114*, 7662−7671.
(24) Seneque, O.; Latour, J.-M. *J. Am. Chem. Soc.* **2010**, *132*, 17760−17774.
(25) Tang, J.; Kang, S.-G.; Saven, J. G.; Gai, F. *J. Mol. Biol.* **2009**, *389*, 90−102.
(26) Seneque, O.; Bonnet, E.; Joumas, F. L.; Latour, J.-M. *Chem.—Eur. J.* **2009**, *15*, 4798−4810.
(27) Li, W.; Zhang, J.; Su, Y.; Wang, J.; Qin, M.; Wang, W. *J. Phys. Chem. B* **2007**, *111*, 13814−13821.
(28) Wise-Scira, O.; Xu, L.; Perry, G.; Coskuner, O. *J. Biol. Inorg. Chem.* **2012**, *17*, 927−938.
(29) Miller, Y.; Ma, B.; Nussinov, R. *Proc. Natl. Acad. Sci. U. S. A.* **2010**, *107*, 9490−9495.
(30) Yang, T.-Y.; Dudev, T.; Lim, C. *J. Am. Chem. Soc.* **2008**, *130*, 3844−3852.
(31) Kuppuraj, G.; Dudev, M.; Lim, C. *J. Phys. Chem. B.* **2009**, *113*, 2952−2960.
(32) Dudev, T.; Lim, C. *Annu. Rev. Biophys.* **2008**, *37*, 97−116.
(33) Alberts, I. L.; Nadassy, K.; Wodak, S. J. *Protein Sci.* **1998**, *7*, 1700−1716.
(34) Elstner, M.; Cui, Q.; Munih, P.; Kaxiras, E.; Frauenheim, T.; Karplus, M. *J. Comput. Chem.* **2003**, *24*, 565−581.
(35) Thomas, P. W.; Zheng, M.; Wu, S.; Guo, H.; Liu, D.; Xu, D.; Fast, W. *Biochemistry* **2011**, *50*, 10102−10113.
(36) Wu, R.; Lu, Z.; Cao, Z.; Zhang, Y. *J. Am. Chem. Soc.* **2011**, *133*, 6110−6113.
(37) Wu, R.; Hu, P.; Wang, S.; Cao, Z.; Zhang, Y. *J. Chem. Theory Comput.* **2010**, *6*, 337−343.
(38) Wu, R.; Wang, S.; Zhou, N.; Cao, Z.; Zhang, Y. *J. Am. Chem. Soc.* **2010**, *132*, 9471−9479.
(39) Kaukonen, M.; Soderhjelm, P.; Heimdal, J.; Ryde, U. *J. Phys. Chem. B* **2008**, *112*, 12537−12548.
(40) Norrby, P. O.; Brandt, P. *Coord. Chem. Rev.* **2001**, *212*, 79−109.

(41) Donini, O. A. T.; Kollman, P. A. *J. Med. Chem.* **2000**, *43*, 4180−4188.
(42) Hoops, S. C.; Anderson, K. W.; Merz, K. M., Jr. *J. Am. Chem. Soc.* **1991**, *113*, 8262−8270.
(43) Vedani, A.; Huhta, D. W. *J. Am. Chem. Soc.* **1990**, *112*, 4759−4767.
(44) Lin, F.; Wang, R. *J. Chem. Theory Comput.* **2010**, *6*, 1852−1870.
(45) Peters, M. B.; Yang, Y.; Wang, B.; Fuesti-Molnar, L.; Weaver, M. N.; Merz, K. M., Jr. *J. Chem. Theory Comput.* **2010**, *6*, 2935−2947.
(46) Dixit, P. D.; Asthagiri, D. *J. Phys. Chem. B* **2011**, *115*, 7374−7382.
(47) Burger, S. K.; Lacasse, M.; Verstraelen, T.; Drewry, J.; Gunning, P.; Ayers, P. W. *J. Chem. Theory Comput.* **2012**, *8*, 554−562.
(48) Pang, Y. P. *J. Mol. Model* **1999**, *5*, 196−202.
(49) Pang, Y. P. *Proteins* **2001**, *45*, 183−189.
(50) Pang, Y. P.; Xu, K.; El Yazal, J.; Prendergast, F. G. *Protein Sci.* **2000**, *9*, 1857−1865.
(51) Pang, Y.-P.; Davis, J.; Wang, S.; Park, J. G.; Nambiar, M. P.; Schmidt, J. J.; Millard, C. B. *PLoS One* **2010**, *5*, e10129.
(52) Pang, Y.-P.; Vummenthala, A.; Mishra, R. K.; Park, J. G.; Wang, S.; Davis, J.; Millard, C. B.; Schmidt, J. J. *PLoS One* **2009**, *4*, e7730.
(53) Stote, R. H.; Karplus, M. *Proteins* **1995**, *23*, 12−31.
(54) Calimet, N.; Simonson, T. *J. Mol. Graphics Modell.* **2006**, *24*, 404−411.
(55) Sakharov, D. V.; Lim, C. *J. Am. Chem. Soc.* **2005**, *127*, 4921−4929.
(56) Sakharov, D. V.; Lim, C. *J. Comput. Chem.* **2009**, *30*, 191−202.
(57) Dal Peraro, M. D.; Spiegel, K.; Lamoureux, G.; De Vivo, M.; DeGrado, W. F.; Klein, M. L. *J. Struct. Biol.* **2007**, *157*, 444−453.
(58) Russell, A. J.; Fersht, A. R. *Nature* **1987**, *328*, 496−500.
(59) Bashford, D.; Karplus, M.; Canters, G. W. *J. Mol. Biol.* **1988**, *203*, 507−510.
(60) Roux, B. *Chem. Phys. Lett.* **1993**, *212*, 231−240.
(61) Lu, Y.; Mei, Y.; Zhang, J. Z. H.; Zhang, D. *J. Chem. Phys.* **2010**, *132*, 131101−131104.
(62) Gresh, N. *J. Comput. Chem.* **1995**, *16*, 856−882.
(63) Tiraboschi, G.; Roques, B. P.; Gresh, N. *J. Comput. Chem.* **1999**, *20*, 1379−1390.
(64) Tiraboschi, G.; Gresh, N.; Giessner-Prettre, C.; Pedersen, L. G.; Deerfield, D. W. *J. Comput. Chem.* **2000**, *21*, 1011−1039.
(65) Garmer, D. R.; Gresh, N. *J. Am. Chem. Soc.* **1994**, *116*, 3556−3567.
(66) Gresh, N.; Stevens, W. J.; Krauss, M. *J. Comput. Chem.* **1995**, *16*, 843−855855.
(67) Gresh, N.; Piquemal, J. P.; Krauss, M. *J. Comput. Chem.* **2005**, *26*, 1113−1130.
(68) Gresh, N.; de Courcy, B.; Piquemal, J.-P.; Foret, J.; Courtiol-Legourd, S.; Salmon, L. *J. Phys. Chem. B* **2011**, *115*, 8304−8316.
(69) de Courcy, B.; Piquemal, J.-P.; Gresh, N. *J. Chem. Theory Comput* **2008**, *4*, 1659−1668.
(70) De Courcy, B.; Gresh, N.; Piquemal, J. P. *Interdiscip. Sci.: Comput. Life Sci.* **2009**, *1*, 55−60.
(71) De Courcy, B.; Dognon, J.-P.; Clavaguera, C.; Gresh, N.; Piquemal, J.-P. *Int. J. Quantum Chem.* **2011**, *111*, 1213−1221.
(72) Antony, J.; Piquemal, J. P.; Gresh, N. *J. Comput. Chem.* **2005**, *26*, 1131−1147.
(73) Wu, J. C.; Piquemal, J.-P.; Chaudret, R.; Reinhardt, P.; Ren, P. *J. Chem. Theory Comput.* **2010**, *6*, 2059−2070.
(74) Li, Y. L.; Mei, Y.; Zhang, D. W.; Xie, D. Q.; Zhang, J. Z. H. *J. Phys. Chem. B* **2011**, *115*, 10154−10162.
(75) Ji, C. G.; Xiao, X.; Zhang, J. Z. H. *J. Chem. Theory Comput.* **2012**, *8*, 2157−2164.
(76) Babu, C. S.; Lim, C. *J. Phys. Chem. A* **2006**, *110*, 691−699.
(77) Diaz, N.; Suarez, D.; Merz, K. M. *Chem. Phys. Lett.* **2000**, *326*, 288−292.
(78) D'Angelo, P.; Barone, V.; Chillemi, G.; Sanna, N.; Meyer-Klaucke, W.; Pavel, N. V. *J. Am. Chem. Soc.* **2002**, *124*, 1958−1967.
(79) Yu, H.; Whitfield, T. W.; Harder, E.; Lamoureux, G.; Vorobyov, I.; Anisimov, V. M.; MacKerell, A. D., Jr.; Roux, B. *J. Chem. Theory Comput.* **2010**, *6*, 774−786.
(80) Obst, S.; Bradaczek, H. *J. Mol. Model.* **1997**, *3*, 224−232.
(81) Fatmi, M. Q.; Hofer, T. S.; Randolf, B. R.; Rode, B. M. *J. Chem. Phys.* **2005**, 123.
(82) Mohammed, A. M.; Loeffler, H. H.; Inada, Y.; Tanada, K.-i.; Funahashi, S. *J. Mol. Liq.* **2005**, *119*, 55−62.
(83) Migliorati, V.; Mancini, G.; Chillemi, G.; Zitolo, A.; D'Angelo, P. *J. Phys. Chem. A* **2011**, *115*, 4798−4803.
(84) Dudev, T.; Lim, C. *Acc. Chem. Res.* **2006**, *40*, 85−93.
(85) Lee, Y.-M.; Lim, C. J. *Am. Chem. Soc.* **2011**, *133*, 8691−8703.
(86) Levy, R.; Sobolev, V.; Edelman, M. *Hum. Mutat.* **2011**, *32*, 1309−1318.
(87) Tiwari, M. K.; Singh, R. K.; Singh, R.; Jeya, M.; Zhao, H.; Lee, J.-K. *J. Biol. Chem.* **2012**, *287*, 19429−19439.
(88) Hong, M.; Fitzgerald, M. X.; Harper, S.; Luo, C.; Speicher, D. W.; Marmorstein, R. *Structure* **2008**, *16*, 1019−1026.
(89) Raha, K.; Merz, K. M. *J. Am. Chem. Soc.* **2004**, *126*, 1020−1021.
(90) Jain, T.; Jayaram, B. *Proteins* **2007**, *67*, 1167−1178.
(91) Raha, K.; Merz, K. M. *J. Med. Chem.* **2005**, *48*, 4558−4575.
(92) Yoshida, T.; Hitaoka, S.; Mashima, A.; Sugimoto, T.; Matoba, H.; Chuman, H. *J. Phys. Chem. B* **2012**, *116*, 10283−10289.
(93) Nicholls, A.; Honig, B. *J. Comput. Chem.* **1991**, *12*, 435−445.